Biophysical Journal
Article

Uncovering the folding mechanism of pertactin: A comparative study of isolated and vectorial folding

Yui Tik Pang,[1] Anthony J. Hazel,[1] and James C. Gumbart[1,*]
[1]School of Physics, Georgia Institute of Technology, Atlanta, GA

ABSTRACT Autotransporters are a large family of virulence factors found in Gram-negative bacteria that play important roles in their pathogenesis. The passenger domain of autotransporters is almost always composed of a large β-helix, with only a small portion of it being relevant to its virulence function. This has led to the hypothesis that the folding of the β-helical structure aids the secretion of the passenger domain across the Gram-negative outer membrane. In this study, we used molecular dynamics simulations and enhanced sampling methods to investigate the stability and folding of the passenger domain of pertactin, an autotransporter from *Bordetella pertussis*. Specifically, we employed steered molecular dynamics to simulate the unfolding of the entire passenger domain as well as self-learning adaptive umbrella sampling to compare the energetics of folding rungs of the β-helix independently ("isolated folding") versus folding rungs on top of a previously folded rung ("vectorial folding"). Our results showed that vectorial folding is highly favorable compared with isolated folding; moreover, our simulations showed that the C-terminal rung of the β-helix is the most resistant to unfolding, in agreement with previous studies that found the C-terminal half of the passenger domain to be more stable than the N-terminal one. Overall, this study provides new insights into the folding process of an autotransporter passenger domain and its potential role in secretion across the outer membrane.

SIGNIFICANCE This study provides new insights into the folding mechanism of the pertactin passenger domain, a key component of *Bordetella pertussis* adhesins that play a major role in the bacteria's pathogenesis. Through the use of advanced simulation techniques, we identified a stable C-terminal hydrophobic core. We also demonstrate that a vectorial folding pathway, in which the domain folds as it crosses the outer membrane, lowers the free energy of folding. Our findings have important implications for our understanding of the structural properties of autotransporter passenger domains and the path dependence of protein folding in general.

INTRODUCTION

Autotransporters are a class of proteins found in Gram-negative bacteria that are typically involved in bacterial virulence. While it was once believed that they contain all the functional elements needed for the secretion of their virulence factors, hence the name, recent research suggests that this may not be entirely true (1–3). Type Va autotransporters consist of two main domains, a C-terminal 12-stranded β-barrel ("β") domain (4–7), which resides in the outer membrane (OM), and an N-terminal β-helical ("passenger") domain (8), which is threaded through the β-barrel and contains the virulence factor itself (9). The mechanism of secretion is still under debate. It is known that passenger domains are secreted unidirectionally from the C- to the N-terminus through the β-barrel (10,11). The secretion of the passenger domain was proposed, with some experimental evidence, to be via a vectorial folding pathway, in which small β-structures form at the C-terminus after secretion that prevent backsliding of the peptide strand through the β-barrel (8,11–13). However, other experiments have challenged this theory, showing both that folding of the passenger domain is not necessary for secretion (14) and that the β-barrel assembly machinery complex orchestrates membrane insertion of the β-barrel and secretion of the passenger domain in a concerted process (10,15–17). Given the absence of ATP or other traditional chemical energy sources at the OM, passenger domain folding itself was attributed as the energy source for secretion. However, one analysis suggests that this folding energy is but a small fraction of the energy required for secretion (14).

The autotransporter pertactin from *B. pertussis*, the causative agent of whooping cough, is a widely studied model of passenger-domain secretion. Studies have shown that

---

Submitted January 29, 2023, and accepted for publication March 14, 2023.

*Correspondence: gumbart@physics.gatech.edu

Yui Tik Pang and Anthony J. Hazel contributed equally to this work.

Editor: Alberto Perez.

https://doi.org/10.1016/j.bpj.2023.03.021

in vitro, the pertactin passenger domain takes several hours to fold and several days to reach equilibrium (8) (Fig. 1). This is much longer than what is expected in vivo, as the typical doubling time of pathogenic bacteria is as short as ∼30–60 min. Furthermore, experiments have revealed that when OM secretion is stalled, the pertactin passenger domain remains unfolded in the periplasm for over 90 min, indicating that secretion and folding of the passenger domain are coupled in vivo (18). A partly folded intermediate state consisting of the first six and a half C-terminal rungs of the β-helix, called the C-terminal core, was observed to be stable on its own and was initially thought be a scaffold for further folding in vivo (8,19). However, the folding rate from this intermediate to the fully folded structure is found to be slower than that from the unfolded state, making the C-terminal core an off-pathway intermediate rather than a scaffold (20). Despite this, the stability of the C-terminal core remains crucial to pertactin secretion (11), with the N-terminal half unable to fold without the presence of the more stable C-terminal half (13). Other proposed mechanisms include an extracellular loop on the β-barrel serving as a scaffold (21,22) and a hydrophobic cavity in the extracellular pore of the β-barrel promoting folding of the passenger domain (21). Overall, the protein folds along a very different pathway during secretion than it does in vitro, and the cellular environment dictates which pathway the protein follows.

Kinetic models predict passenger domain folding to be the driving force for secretion efficiency (18). Studies have shown that destabilizing the N-terminus of the passenger domain improves efficiency, while destabilizing the C-terminus has the opposite effect (12,13,23,24). These results imply that a free energy gradient along the passenger domain β-helix is important for efficient secretion. This free energy gradient could serve several purposes: 1) to prevent folding during secretion across the inner membrane into the periplasm, which proceeds in the opposite direction of OM secretion, 2) to slow the formation of the native state while in the periplasm, and 3) to facilitate the faster, vectorial process during OM secretion into the extracellular space.

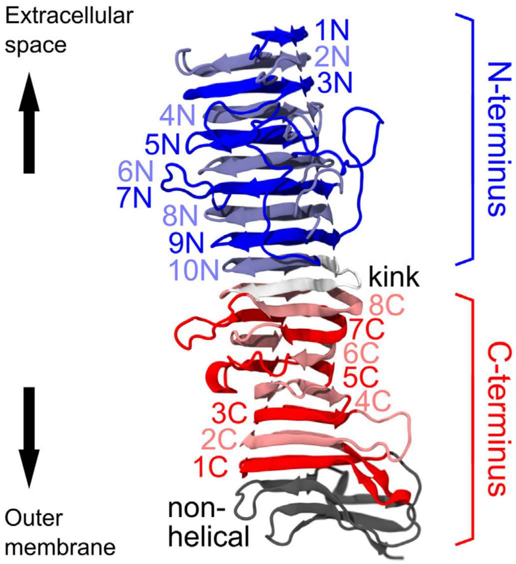

FIGURE 1 Crystal structure of the pertactin passenger domain from *B. pertussis* (PDB: 1DAB). The structure is colored and labeled by rungs, with each band representing two consecutive rungs, named after the rung closest to the termini (e.g., rungs 1C and 2C form band 1C). To see this figure in color, go online.

In this study, we use steered molecular dynamics (SMD) simulations to gain insight into the folding process of the pertactin passenger domain by unfolding it instead. Additionally, we employ enhanced sampling methods to compare the energetics of the in vitro and in vivo folding pathways of the pertactin passenger domain in order to assess the efficacy of vectorial folding as the energy source for secretion.

MATERIALS AND METHODS

System construction

The pertactin β-helical passenger domain structure was taken from PDB: 1DAB (25). Here, a “rung” refers to 2–3 connecting β-strands that complete a turn in the β-helix, and a “band” refers to two successive rungs, e.g., band 1C refers to the first two rungs at the C-terminus of the β-helix (Fig. 1). CHARMM22* (26) parameters were chosen to describe the protein, which we have previously shown to accurately describe β-hairpin folding (27).

The SMD simulations were carried out in four separate segments due to the size of the protein, each with a different part of the passenger domain present, namely the N-terminus to rung 10N (D1–G284), rung 8N to rung 5C (A184–G391), rung 10N to the C-terminus (Y262–P539), and rung 4C to the C-terminus (V396–P539). The protein segments were then solvated in 13.5 × 8 × 8, 13.5 × 8 × 8, 15 × 7 × 7, and 16.8 × 7 × 7 nm boxes of TIP3P water molecules (28), respectively. The systems were neutralized with 0.15 M NaCl. The system sizes ranged from ∼70,000 to ∼106,000 atoms. All C_α atoms of the first band at the C-terminal end of each system were restrained to their positions in the crystal structure (Table S1).

To measure the folding potentials of mean force (PMFs) for isolated bands, we isolated each band from the rest of the structure. Table S2 details which residues were used for each system. Each peptide was then solvated in a 15 × 7 × 7 nm box with ∼23,000 TIP3P water molecules (28) and neutralized with 0.15 M NaCl, for a total system size of ∼70,000 atoms. To align the end-to-end vector of the peptide along the x axis, we applied further restraints using the distanceXY function from the colvars module of NAMD (29) to ensure that the distance between the first and last residues of the peptide along the y and z axes was zero. The force constant of this restraint was set to 1000 kcal/mol nm^2.

For vectorial folding PMFs of each band, we constructed systems that also included all residues C-terminal to that band, stopping at residue 280 for band 1N and residue 539 for band 2C. Each system was solvated in a water box with lengths chosen to accommodate the peptide with a fully unfolded and extended N-terminal rung. This resulted in box lengths of ∼6.5–8 nm for the y and z dimensions and ∼11.7–19.3 nm for the x dimension. Each system was also neutralized with 0.15 M NaCl. Total system sizes ranged from ∼53,000 to 106,000 atoms. The heavy backbone atoms of all β-sheet residues not in the first N-terminal rung were restrained to their native conformations.

MD simulations

MD simulations were carried out using NAMD 2.10–12 (30). The temperature was held at 310 K using Langevin dynamics; the pressure was kept constant at 1 atm using the Langevin piston method (31). The equations of motion were integrated using the RESPA multiple time-stepping algorithm with a time step of 2 fs used for all bonded interactions, 2 fs for short-range nonbonded interactions, and 4 fs for long-range electrostatic interactions. Long-range electrostatic interactions were calculated using the particle-mesh Ewald method with a real-space cutoff of 1.2 nm (32). Short-range, non-bonded Lennard-Jones interactions were cut off at 1.2 nm with a potential switching function beginning at 1 nm bringing the potential energy smoothly to zero at the cutoff distance. Bonds involving hydrogen atoms were constrained to their equilibrium length, employing the SETTLE algorithm (33) for water molecules and the SHAKE algorithm for all others (34).

SMD

SMD was applied to the first C_α atom at the N-terminal end of each system at a speed of 0.1 nm/ns in the +x direction with a force constant of 500 kcal/mol nm^2. The passenger domain was prealigned to the x axis so that the force pulled the N-terminal C_α away from the C-terminus. The simulation was repeated three times for each segment of the passenger domain. The protein was trimmed every 40–100 ns to ensure the extended portion of the protein did not interact with its periodic image. The N-terminus to rung 10N, rung 8N to rung 5C, rung 10N to C-terminus, and rung 4C to C-terminus systems were pulled for 540–560, 220, 400, and 260 ns, respectively. The total distances pulled for each run varied slightly due to the difference in length of the trimmed parts.

Self-learning adaptive umbrella sampling procedure

Two-dimensional folding free energy landscapes of the β-helical bands of pertactin were calculated using umbrella sampling (US). Our two reaction coordinates are similar to those previously used for the β-hairpin peptide GB1 (27), namely the number of native H-bonds along the β-sheets (N_{hb}) and the radius of gyration for all internal hydrophobic side chains (R_{G}). The N_{hb} coordinate is the sum of individual hydrogen bond collective variables, defined by Eq. 1.

$$\mathrm{hbf}(\mathrm{donor}, \mathrm{acceptor}) = \frac{1 - \left(|x_{\mathrm{don}} - x_{\mathrm{acc}}|/d_0\right)^6}{1 - \left(|x_{\mathrm{don}} - x_{\mathrm{acc}}|/d_0\right)^8}, \qquad (1)$$

This hbf function is a smooth function from 0 to 1 where hbf $\approx$ 1 if two atoms are well within the cutoff ($d_0 = 0.33$ nm) and where hbf $\approx$ 0 when they are well outside the cutoff. Windows were spaced by 0.25 along N_{hb}, with a harmonic force constant of 25.0 kcal/mol, and by 0.05 nm along R_{G}, with a harmonic force constant of 625 kcal/mol nm^2. All US simulations were run at 310 K. PMFs were generated via the weighted histogram analysis method (35,36).

To initiate the self-learning adaptive US (SLUS) procedure (37,38) for the isolated bands, we first ran a 10 ns simulation at 310 K followed by another 10 ns simulation at 500 K. From these simulations, we generated starting states for a 2D US simulation. We used a 5 kcal/mol free energy cutoff for our SLUS procedure, with 2 ns/window simulations for each iteration. We used replica-exchange US (REUS) (39) for the initial set of windows (iteration 0) and normal US for all subsequent iterations. Upon completion of the SLUS procedure, we then ran 10 ns/window of REUS on all generated windows. Table S2 tabulates the number of SLUS iterations and the number of generated windows for each band.

For the vectorial folding PMFs, we used ~50–150 ns metadynamics simulations (40) for each system to generate 333 and 210 windows for bands 1N and 2C, respectively. We ran an initial 7 and 5 ns/window of REUS simulations for bands 1N and 2C, respectively, using the final 5 ns/window to calculate initial PMFs. Initial reaction coordinate coverage from the metadynamics simulations was sufficient such that SLUS did not yield additional exploration of the reaction coordinate space. To check convergence for band 2C, we ran an additional 5 ns/window of REUS simulations, which did not yield a difference in the PMF beyond the numerical accuracy.

RESULTS

The C-terminus possesses a stable hydrophobic core

To investigate the folding of the pertactin passenger domain, we simulated the reverse process and unfolded the protein using SMD simulations. A pulling force with a force constant of 500 kcal/mol nm^2 was applied at the N-terminal C_α, moving it away from the C-terminus at a constant speed of 0.1 nm/ns. The C-terminal band was held in place by fixing all of its C_αs. The simulation was repeated three times. Because of the large size of the passenger domain, the pulling process was divided into four individual runs with only a fraction of the whole protein present in the simulation (see materials and methods). The unfolded part of the protein was also removed periodically to prevent it from extending beyond the periodic boundary. We correlated each force spike recorded during the simulation to its corresponding unfolding event (see supporting material), and a few are described in more detail below.

In all three replicas of the SMD simulation, the pertactin passenger domain generally unfolds strand by strand from the N- to the C-terminus (Video S1), despite the absence of explicit restraints on the unfolding order of the protein. Fig. 2 *A* illustrates the resistance force profile obtained during unfolding of the protein. A number of force spikes were observed, with each of them indicating the breaking of a β-strand from the β-helix. The force spike at a pulled distance of ~130 nm, however, stands out, as it exhibits the highest peak force, the largest area under the F-x curve, and is consistently observed across all three replicas. This spike is recorded during the unfolding of the β-hairpin at V454–S461, which connects the first two rungs at the C-terminus (rungs 1C and 2C, or band 1C) and interfaces with the non-β-helical C-terminal region. This β-hairpin is the only connecting loop between rungs that is structured. It is also the only β-hairpin in the pertactin passenger domain other than the non-β-helical C-terminal region. The composition of this β-hairpin is dominated by hydrophobic residues (Fig. 2 *D*), and it is sandwiched between two unstructured loops in the folded structure, protecting it from exposure to the aqueous environment. Previous studies have shown that the C-terminus of the pertactin passenger domain forms a stable hydrophobic core and is resistant to proteinase K digestion (19). Our results are in agreement with these experimental findings and pinpoint the center of this hydrophobic core to be the V454–S461 β-hairpin. It is worth noting that a stable C-terminus is not unique to the passenger domain of pertactin but is consistently found in many type Va autotransporters, such as Pet (19), supporting the vectorial folding hypothesis of autotransporter secretion (19,24).

We further analyzed the SMD simulations to determine the underlying causes of the large force spike observed during

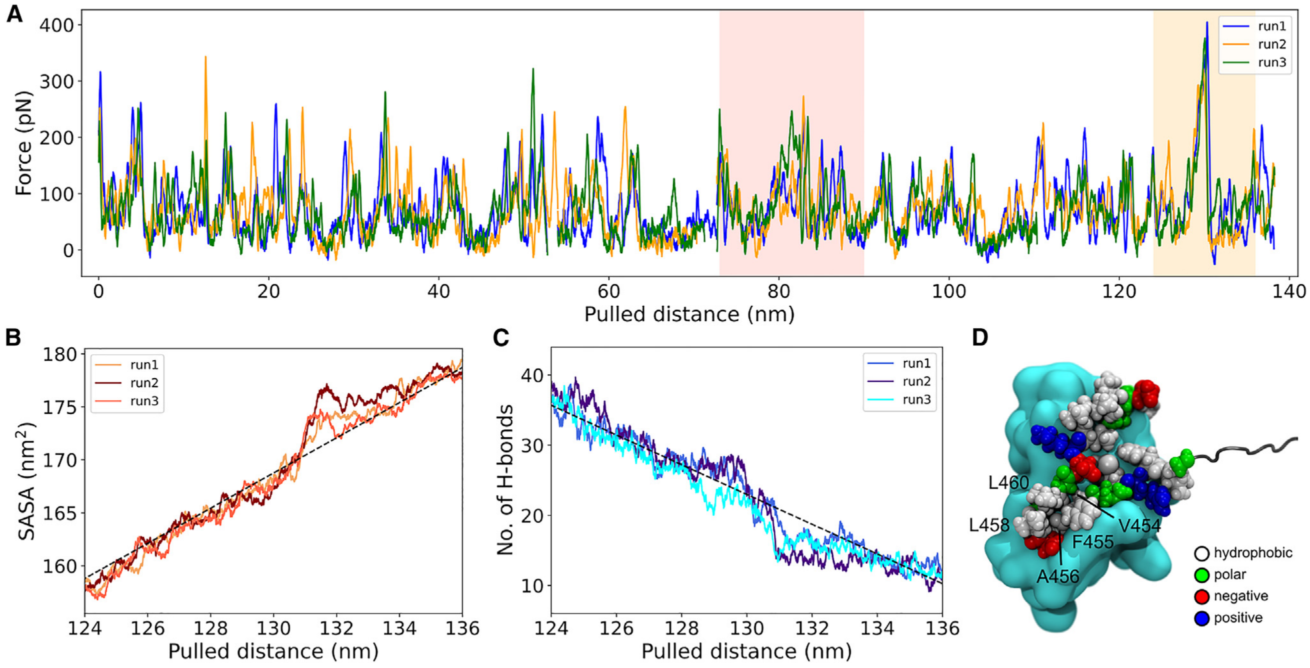

FIGURE 2 SMD simulation results of the unfolding of the pertactin passenger domain. (*A*) Force-distance profiles for all three replicas of the simulation. The rungs of the β-helix unfold one by one from the C- to the N-terminus throughout the simulation except when unfolding the kink (*pale red*, see Fig. 3). The force spike observed near the end of the simulation at a pulled distance of ~130 nm (*pale orange*) is consistently observed across all replicas and corresponds to the unfolding of the β-hairpin at V454–S461. (*B*) Solvent-accessible surface area of the hydrophobic residues and (*C*) number of H-bonds against the pulled distance over the pale orange shaded region. A sharp increase in solvent-accessible surface area and decrease in H-bonds are observed at the same point as the force spike in (*A*). (*D*) Snapshot from the SMD simulations before the β-hairpin unfolds. The residues of band 1C are colored by their residue types, with hydrophobic, polar, negatively charged, and positively charged residues colored as white, green, red, and blue, respectively. To see this figure in color, go online.

the unfolding of band 1C. Our analysis revealed that a sharp increase in the solvent-accessible surface area (SASA) of the hydrophobic residues occurred (Fig. 2 *B*), as well as a sharp drop of ~5 H-bonds (Fig. 2 *C*) right after the unfolding of β-hairpin V454–S461. The observation reveals that the extra resistance to unfolding of the β-hairpin is due to two factors: the breaking of all H-bonds between the hairpin at once, rather than one by one as in unfolding the rungs, and the simultaneous exposure of five hydrophobic residues to the solvent (Fig. 2 *D*). These physical factors provide the basis for the large force spike observed in all three replicas.

At the other end of the β-helix, we also observed a consistent force spike when unfolding the first and second rungs at the N-terminus (rungs 1N and 2N or band 1N) at pulled distances of 0 and 5 nm, respectively (Fig. 2 *A*). The spike suggests that band 1N may play a role in capping the β-helix and preventing aggregation at this end of the passenger domain (41).

A kinked rung resists unfolding

SMD simulation results across all three replicas show that the pertactin passenger domain unfolds in a strand-by-strand manner, with the only exception occurring when the kink (I277–R291) is pulled off at a distance of ~80 nm. The kink, located in the middle of the passenger domain, creates a slight orientation change of around 20° between the C- and N-terminal halves. In runs 1 and 2, the β-strand adjacent to the kink from the next rung (A304–G314) detached from the rest of the folded structure and unfolded along with the kink (Fig. 3 *A*). In run 3, an even larger portion of the protein detached, resulting in a rupture between rungs 5C (P378–G391) and 6C (P348–V364) (Fig. 3 *B*). All three runs exhibited a significant force spike >200 pN tall and ~6 nm wide during the detachment (Fig. 2 *A*), accompanied by a drop of ~8 total H-bonds (Fig. 3 *C*).

There are several factors contributing to this multistrand detachment, one of which is the unique arrangement of the charged residues around the kink. The positively charged residue R288 on the kink interacts strongly with two negatively charged residues on the two adjacent rungs, namely D265 and E311 (Fig. S1 *B*). Furthermore, solvent-accessible surface area calculations revealed that D265 and E311 are among the top four charged residues with the least exposure to the solvent (Fig. S1 *A*), further stabilizing their electrostatic interactions within the β-helix. In particular, the interaction between R288 and E311 was maintained even after both of their rungs had unfolded in runs 1 and 2 (Fig. 3 *A*). Instead, rung 8C detached from the rest of the β-helix to maintain contact with the kink until it became too distant, and all possible interactions between them were eliminated. Previous experimental

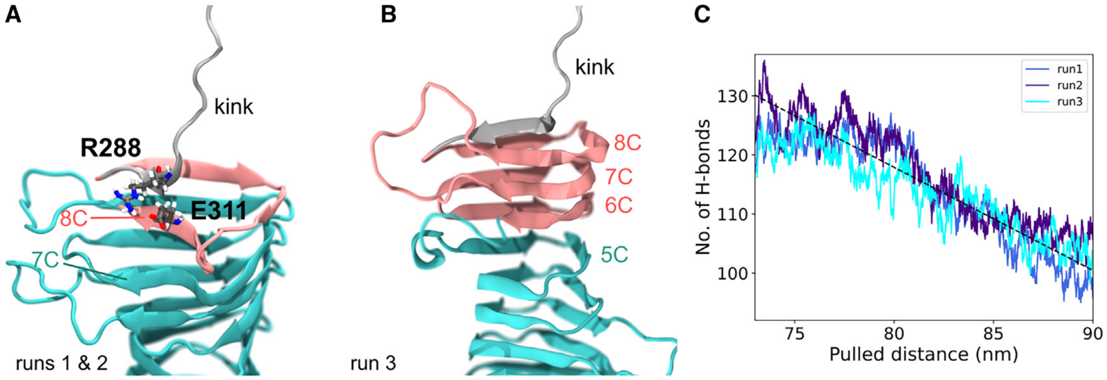

FIGURE 3 Unique unfolding mechanism when the kink is being pulled off. (*A* and *B*) The pertactin passenger domain unfolds strand by strand throughout the SMD simulation except when the kink (I277–R291, *silver*) unfolds. (*A*) In runs 1 and 2, an adjacent β-strand (A304–G314, *pink*) detaches along with the kink, partly due to the strong electrostatic interactions between the positively charged residue R288 on the kink and the negatively charged residue E311. (*B*) In run 3, an even larger portion of the protein (rungs 6C–8C, *pink*) detaches. (*C*) The events are accompanied by a drop of ~8 H-bonds, explaining the strong resistance force as seen in Fig. 2 *A*. To see this figure in color, go online.

studies have identified the stable C-terminal structural core as A335–P539, which encompasses the passenger domain from the C-terminus to rung 7C (8), matching the point of rupture observed in our SMD simulation runs 1 and 2.

Another important factor for the multistrand detachment, highlighted by run 3, is the geometry of the passenger domain, which has its C-terminal half roughly resembling the shape of a boot. The kink (the top of the "boot") has a larger cross-sectional area than the rungs down the "shaft," providing a larger hydrophobic core and allowing more H-bonds between the backbones of the rungs, with both strengthening its structural integrity. As the kink is being pulled, the shaft effectively transfers the pulling force to the structural weak point of the boot, disrupting the structure at a point with a small cross-sectional area, i.e., between rungs 5C and 6C.

Overall, our results indicate that the kink is more stable than the band composed of rungs 5C and 6C as well as that composed of rungs 7C and 8C, leading to these two bands breaking before the kink unfolds. One functional benefit of having a more stable kink structure could be to facilitate the secretion of the long loop connecting rungs 9N and 10N (R226–W261), which contains the RGD motif for cell adhesion (42) (Fig. 1).

Instability of isolated bands revealed through potentials of mean force

We employed SLUS (see materials and methods) (37) to explore the folding free energy landscapes of individual isolated bands taken from the pertactin β-helical passenger domain (see Fig. 1 for the definition of the bands). Specifically, we focused on the first three bands at the C- and N-termini, as well as the central kinked band consisting of two full rungs with one incomplete rung between them (see Table S2 and Fig. 1). We used the same reaction coordinates as those used in previous studies for the GB1 β-hairpin (27) (see materials and methods). Upon completion of the SLUS procedure, 10 ns/window of REUS was performed on all generated windows. The resulting 2D-folding PMFs are shown in Fig. 4 *A* and Fig. S2.

The native state of each band is unstable in isolation. In some cases, namely bands 1C and 3N, the native state was not captured by the SLUS procedure. These bands quickly lost the native structure within the first nanosecond of the initial 310 K equilibrium simulations, and the energy barrier to refold them was too large for the SLUS procedure to overcome with only a 5 kcal/mol cutoff. For the remaining bands, only bands 3C and 2N possess a free energy minimum near the native state. Band 1C is the only other band to have a minimum outside of the unfolded regime, with two minima at ~3.5 and ~8.5 H-bonds, and all minima are separated by barriers of <2 kcal/mol. Band 2N also exhibits intermediate folded states between 5 and 8 H-bonds, with minima separated by barriers of <3 kcal/mol.

Among all the bands we examined, band 1C has the highest stability. Analysis of the PMFs shows that band 1C has three states that exist in roughly equal proportions: one fully unfolded state and two partially folded states. Combining the two partially folded states results in a folding free energy (ΔG_{fold}) of -0.8 ± 0.5 kcal/mol, indicating that the band is in a partially folded state for ~79% of the time. When considering only the most structured minimum, which is ~60% folded by the number of native H-bonds preserved, ΔG_{fold} increases to $+0.2 \pm 0.4$ kcal/mol, with the percentage of time spent in the partially folded state decreasing to ~44%. The band with the second highest stability after band 1C is band 2N. It has three minima: one fully unfolded, one partially folded (~40%–60%), and the fully folded native state. Combining the two folded states results in a ΔG_{fold} of $+0.7 \pm 0.6$ kcal/mol, with native structure present ~25% of the time. Restricting to only the native-state minimum, these two values changes to $+1.7 \pm 1.1$ kcal/mol and ~6%, respectively. The band with the next highest percentage of any observed native structure is band 3C at only

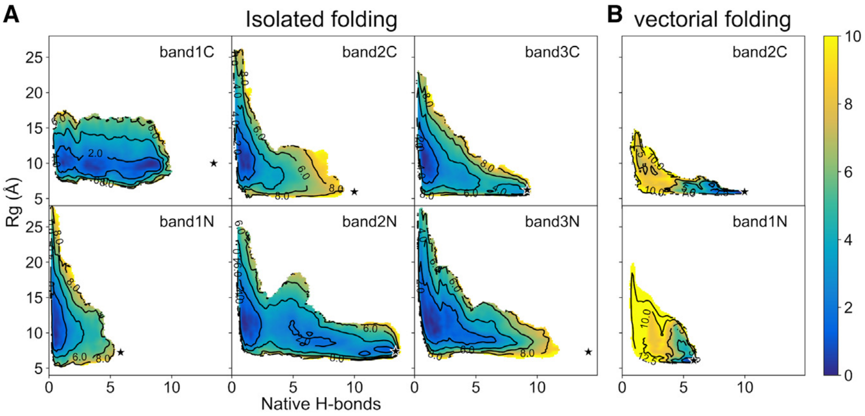

FIGURE 4 PMFs for the folding of pertactin passenger domain bands. (*A*) 2D PMFs for isolated folding of bands 1–3C and 1–3N along two collective variables, N_{hb} and R_G, showing the native structures (indicated with a *star*) are unstable except for bands 1C and 2N. (*B*) 2D PMFs for vectorial folding of bands 2C and 1N along the same variables, showing that the native structures become highly favorable. To see this figure in color, go online.

~0.7%. All other bands have any native structure present for <0.1% of the time.

Our PMFs indicate clearly that the majority of the bands of the β-helix are unable to fold on their own without the support of neighboring structures. However, band 1C stands out as the most stable among all the bands and is able to partially fold on its own. This finding is consistent with the results from our SMD simulations, which also highlight band 1C as the most difficult band to unfold. Our results support the hypothesis that band 1C plays a key role in the folding process, as previously suggested by experiments (8,13). The slow folding rate observed in vitro (8) can also be explained by the lack of stability in isolation for the majority of the bands. On the N-terminal side, band 2N shows a substantial native structure population, pointing to its potential role as a "capping" mechanism to prevent aggregation of the β-helix (41), as similarly supported by our SMD results.

Vectorial folding stabilizes the β-helical bands

The vectorial folding free energy landscapes for bands 2C and 1N were calculated by restraining all C-terminal β-strands to their native conformations while only allowing the most N-terminal rung to move freely (see materials and methods for more details). Their PMFs are shown in Fig. 4 *B*.

In contrast to the instability observed when isolated (Fig. 4 *A*), these bands (2C and 1N) exhibit high stability (around − 10 kcal/mol) when folding on top of their adjacent C-terminal bands, as would occur during vectorial folding. The sharp decrease in entropy due to the restraints on one of the two rungs in the band contributes to a significant increase in relative free energy for the unfolded state.

In the vectorial folding hypothesis, during OM secretion, only small sections of the peptide immediately N-terminal to the already secreted and folded bands of the β-helix are believed to be in the extracellular space, while the remaining peptide wriggles freely on the periplasmic side. The entropy of the periplasmic portion is likely even higher than that in our truncated isolated systems, so the increase in the free energy of the unfolded state could be significantly larger than observed here, further stabilizing the folded states on the extracellular side. The vectorial pathway not only prevents backsliding of the peptide across the OM, but it also eliminates the barrier for folding and significantly stabilizes the folded state in the process.

DISCUSSION

In this study, we aimed to gain a deeper understanding of the folding mechanism of the passenger domain of pertactin, an adhesin in *B. pertussis* that contributes to the bacteria's pathogenesis. To achieve this goal, we employed a combination of different computational techniques, including SMD, SLUS, and REUS simulations, to investigate the stability and folding of the different bands of the pertactin passenger domain. By holding the C-terminal band fixed and pulling on the N-terminal end, the pertactin passenger unfolds strand by strand in our SMD simulations from the N- to the C-terminus, with the exception of a kink located at the middle. Results from the SMD simulations showed that band 1C had the highest resistance to unfolding, which is consistent with previous studies that have identified a stable C-terminal hydrophobic core (8,19). In particular, the force is the highest when unfolding the β-hairpin (V454–S461) in band 1C, which connects rungs 1C and 2C and rests on a hydrophobic region of the non-β-helical C-terminus. This unfolding process requires the simultaneous breaking of all hydrogen bonds within the β-hairpin and the exposure of a large number of hydrophobic residues to the solvent, resulting in its high resistance to unfolding.

Our SMD simulations provide insight into the unfolding behavior of the pertactin passenger domain, while our SLUS and REUS simulations reveal the folding energetics of individual bands. Analysis of the PMFs shows that folding in isolation is energetically unfavorable for most bands, with band 1C being the only exception, exhibiting a negative ΔG_{fold} of -0.8 ± 0.5 kcal/mol. Both simulation approaches, SMD and REUS, consistently demonstrate that band 1C is uniquely stable, suggesting a possible role as the folding nucleus of the passenger domain.

While the folding of band 2N in isolation is unfavorable, with a ΔG_{fold} of $+0.7 \pm 0.6$ kcal/mol, it is the only other band (in addition to band 1C) that has a significant population (~25%) in its native structure. Our results suggest that the two terminal bands may act as scaffolds for the propagation of β-helical structure inward toward the kinked region, giving rise to the concerted folding process observed for the pertactin passenger domain in vitro (20). Additionally, our results show that the vectorial folding pathway significantly stabilizes the native state of bands 2C and 1N by providing a template for each successive rung to fold.

In conclusion, our study sheds light on the folding mechanism and stability of the pertactin passenger domain, which serves as an archetype for type Va autotransporters. Our findings also elucidate the structural properties of this particular protein, which likely contribute to the virulence of *B. pertussis*. These properties may be useful for the development of new vaccines and therapeutics against pertussis by targeting the vectorial folding pathway. For example, inhibiting folding and secretion of pertactin could limit virulence while minimizing the potential risk for evolved resistance.

SUPPORTING MATERIAL

Supporting material can be found online at https://doi.org/10.1016/j.bpj.2023.03.021.

AUTHOR CONTRIBUTIONS

J.C.G. designed the research. Y.T.P. and A.J.H. carried out all simulations and analyzed the data. Y.T.P., A.J.H., and J.C.G. wrote the article.

ACKNOWLEDGMENTS

This work was supported by the National Institutes of Health (R01-GM123169). Computational resources were provided through the Extreme Science and Engineering Discovery Environment (TG-MCB130173), which is supported by the National Science Foundation (ACI-1548562). This work also used the Hive cluster, which is supported by the National Science Foundation (MRI-1828187) and is managed by the Partnership for an Advanced Computing Environment (PACE) at GT.

DECLARATION OF INTERESTS

The authors declare no competing interests.

REFERENCES

1. Sauri, A., Z. Soprova, …, J. Luirink. 2009. The Bam (Omp85) complex is involved in secretion of the autotransporter haemoglobin protease. *Microbiology.* 155:3982–3991.
2. Wu, R., J. W. Bakelar, …, N. Noinaj. 2021. Plasticity within the barrel domain of BamA mediates a hybrid-barrel mechanism by BAM. *Nat. Commun.* 12:7131.
3. Kuo, K. M., D. Ryoo, …, J. C. Gumbart. 2022. Modeling intermediates of BamA folding an outer membrane protein. *Biophys. J.* 121:3242–3252.
4. Oomen, C. J., P. van Ulsen, …, P. Gros. 2004. Structure of the translocator domain of a bacterial autotransporter. *EMBO J.* 23:1257–1266.
5. Barnard, T. J., N. Dautin, …, S. K. Buchanan. 2007. Autotransporter structure reveals intra-barrel cleavage followed by conformational changes. *Nat. Struct. Mol. Biol.* 14:1214–1220.
6. van den Berg, B. 2010. Crystal structure of a full-length autotransporter. *J. Mol. Biol.* 396:627–633.
7. Meuskens, I., A. Saragliadis, …, D. Linke. 2019. Type V secretion systems: an overview of passenger domain functions. *Front. Microbiol.* 10:1163.
8. Junker, M., C. C. Schuster, …, P. L. Clark. 2006. Pertactin β-helix folding mechanism suggests common themes for the secretion and folding of autotransporter proteins. *Proc. Natl. Acad. Sci. USA.* 103:4918–4923.
9. Leyton, D. L., A. E. Rossiter, and I. R. Henderson. 2012. From self sufficiency to dependence: mechanisms and factors important for autotransporter biogenesis. *Nat. Rev. Microbiol.* 10:213–225.
10. Ieva, R., and H. D. Bernstein. 2009. Interaction of an autotransporter passenger domain with BamA during its translocation across the bacterial outer membrane. *Proc. Natl. Acad. Sci. USA.* 106:19120–19125.
11. Junker, M., R. N. Besingi, and P. L. Clark. 2009. Vectorial transport and folding of an autotransporter virulence protein during outer membrane secretion. *Mol. Microbiol.* 71:1323–1332.
12. Peterson, J. H., P. Tian, …, H. D. Bernstein. 2010. Secretion of a bacterial virulence factor is driven by the folding of a C-terminal segment. *Proc. Natl. Acad. Sci. USA.* 107:17739–17744.
13. Renn, J. P., M. Junker, …, P. L. Clark. 2012. ATP-independent control of autotransporter virulence protein transport via the folding properties of the secreted protein. *Chem. Biol.* 19:287–296.
14. Kang'ethe, W., and H. D. Bernstein. 2013. Charge-dependent secretion of an intrinsicially disordered protein via the autotransporter pathway. *Proc. Natl. Acad. Sci. USA.* 110:E4246–E4255.
15. Ieva, R., P. Tian, …, H. D. Bernstein. 2011. Sequential and spatially restricted interactions of assembly factors with an autotransporter β domain. *Proc. Natl. Acad. Sci. USA.* 108:E343–E391.
16. Pavlova, O., J. H. Peterson, …, H. D. Bernstein. 2013. Mechanistic link between β barrel assembly and the initiation of autotransporter secretion. *Proc. Natl. Acad. Sci. USA.* 110:E938–E947.
17. Ryoo, D., M. O. Rydmark, …, J. C. Gumbart. 2020. BamA is required for autotransporter secretion. *Biochim. Biophys. Acta. Gen. Subj.* 1864:129581.
18. Drobnak, I., E. Braselmann, and P. L. Clark. 2015. Multiple driving forces required for efficient secretion of autotransporter virulence proteins. *J. Biol. Chem.* 290:10104–10116.
19. Renn, J. P., and P. L. Clark. 2008. A conserved stable core structure in the passsenger domain β-helix of autotransporter virulence proteins. *Biopolymers.* 89:420–427.
20. Junker, M., and P. L. Clark. 2010. Slow formation of aggregation-resistant β-sheet folding intermediates. *Proteins.* 78:812–824.
21. Zhai, Y., K. Zhang, …, F. Sun. 2011. Autotransporter passenger domain secretion requires a hydrophobic cavity at the extracellular entrance of the β-domain pore. *Biochem. J.* 435:577–587.
22. Yuan, X., M. D. Johnson, …, D. L. Leyton. 2018. Molecular basis for the folding of β-helical autotransporter passenger domains. *Nat. Commun.* 9:1395.
23. Besingi, R. N., J. L. Chaney, and P. L. Clark. 2013. An alternative outer membrane secretion mechanism for an autotransporter lacking a C-terminal stable core. *Mol. Microbiol.* 90:1029–1045.
24. Braselmann, E., and P. L. Clark. 2012. Autotransporters: the cellular environment reshapes a folding mechanism to promote protein transport. *J. Phys. Chem. Lett.* 3:1063–1071.

25. Emsley, P., I. G. Charles, …, N. W. Isaacs. 1996. Structure of *Bordetella pertussis* virulence factor P.69 pertactin. *Nature.* 381:90–92.
26. Piana, S., K. Lindorff-Larsen, and D. E. Shaw. 2011. How robust are protein folding simulations with respect to force field parametrization? *Biophys. J.* 100:L47–L49.
27. Hazel, A. J., E. T. Walters, …, J. C. Gumbart. 2018. Folding free energy landscapes of β-sheets with non-polarizable and polarizable CHARMM force fields. *J. Chem. Phys.* 149:072317.
28. Jorgensen, W. L., J. Chandrasekhar, …, M. L. Klein. 1983. Comparison of simple potential functions for simulating liquid water. *J. Chem. Phys.* 79:926–935.
29. Fiorin, G., M. L. Klein, and J. Hénin. 2013. Using collective variables to drive molecular dynamics simulations. *Mol. Phys.* 111:3345–3362.
30. Phillips, J. C., R. Braun, …, K. Schulten. 2005. Scalable molecular dynamics with NAMD. *J. Comput. Chem.* 26:1781–1802.
31. Feller, S. E., Y. Zhang, …, B. R. Brooks. 1995. Constant pressure molecular dynamics simulations — the Langevin piston method. *J. Chem. Phys.* 103:4613–4621.
32. Darden, T., D. York, and L. Pedersen. 1993. Particle mesh Ewald: an *N* log *N* method for Ewald sums in large systems. *J. Chem. Phys.* 98:10089–10092.
33. Miyamoto, S., and P. A. Kollman. 1992. Settle: an analytical version of the SHAKE and RATTLE algorithm for rigid water models. *J. Comput. Chem.* 13:952–962.
34. Ryckaert, J.-P., G. Ciccotti, and H. J. Berendsen. 1977. Numerical integration of the cartesian equations of motion of a system with constraints: molecular dynamics of *n*-alkanes. *J. Comput. Phys.* 23:327–341.
35. Kumar, S., J. M. Rosenberg, …, P. A. Kollman. 1992. The weighted histogram analysis method for free-energy calculations on biomolecules. I. The method. *J. Comput. Chem.* 13:1011–1021.
36. Grossfield, A.. WHAM: the weighted histogram analysis method, version 2.0.6. http://membrane.urmc.rochester.edu/content/wham.
37. Wojtas-Niziurski, W., Y. Meng, …, S. Bernèche. 2013. Self-learning adaptive umbrella sampling method for the determination of free energy landscapes in multiple dimensions. *J. Chem. Theory Comput.* 9:1885–1895.
38. Hazel, A. J., N. Abdali, …, J. C. Gumbart. 2019. Conformational dynamics of AcrA govern multidrug efflux pump assembly. *ACS Infect. Dis.* 5:1926–1935.
39. Sugita, Y., A. Kitao, and Y. Okamoto. 2000. Multidimensional replica-exchange method for free-energy calculations. *J. Chem. Phys.* 113:6042–6051.
40. Laio, A., and M. Parrinello. 2002. Escaping free-energy minima. *Proc. Natl. Acad. Sci. USA.* 99:12562–12566.
41. Bryan, A. W., Jr., J. L. Starner-Kreinbrink, …, B. Berger. 2011. Structure-based prediction reveals capping motics that inhibit β-helix aggregation. *Proc. Natl. Acad. Sci. USA.* 108:11099–11104.
42. Everest, P., J. Li, …, M. Roberts. 1996. Role of the Bordetella pertussis P.69/pertactin protein and the P.69/pertactin RGD motif in the adherence to and invasion of mammalian cells. *Microbiology.* 142:3261–3268.